Astron. Astrophys. 338, 661–673 (1998)

ASTRONOMY AND ASTROPHYSICS

# Photospheric metal abundances in active stellar atmospheres

**R. Ottmann**[1], **M.J. Pfeiffer**[2], **and T. Gehren**[2]

[1] Max-Planck-Institut für Extraterrestrische Physik, D-85748 Garching, Germany
[2] Institut für Astronomie und Astrophysik der Universität München, Scheinerstrasse 1, D-81679 München, Germany

Received 9 April 1998 / Accepted 8 July 1998

**Abstract.** With a sophisticated analysis we determine the photospheric metal abundances of active stars to investigate the abundance stratification in active stellar atmospheres. For selected single stars and RS CVn binaries we have taken high-resolution, high-SN and partially phase-resolved spectra of the entire visible range. With a purely spectroscopic, self-consistent method based on line profile synthesis and an equivalent width analysis, we derive the effective temperature $T_{eff}$, surface gravity $\log g$, microturbulence $\xi_t$ and the abundances of Fe, Mg and Si with high internal accuracy ($\Delta T_{eff} \simeq 70\,\mathrm{K}$, $\Delta \log g \simeq 0.1\,\mathrm{dex}$, $\Delta\xi_t \simeq 0.1\,\mathrm{km/s}$, $\Delta[\mathrm{Fe/H}], \Delta[\mathrm{Mg/H}], \Delta[\mathrm{Si/H}] \simeq 0.05\,\mathrm{dex}$). Stellar parameters and metal abundances are obtained for the single stars $\beta$ Cet, $\kappa$ Cet and $\pi^1$ UMa as well as for the RS CVn binaries AY Cet, VY Ari, EI Eri, IM Peg, $\lambda$ And and II Peg. The effect of stellar activity features (spots and plages) on the derived parameters is investigated by phase-resolved spectroscopy; we find that one out of four systems shows a significant variation of the Mg and Si abundances with rotational phase. The results help solving the puzzle about the photospheric Fe abundances of RS CVn binaries; specifically, we obtain $[\mathrm{Fe/H}] \geq -0.4$ for all systems, indicating that they definitely are not metal-poor. In II Peg and $\lambda$ And, the metals are strongly depleted in the corona relative to the photosphere; in $\beta$ Cet and $\pi^1$ UMa, Fe and Si are weakly depleted, but Mg is enhanced (with $1\sigma$ significance). The abundance stratifications are discussed in terms of the FIP-effect and the hydrostatic equilibrium stratification.

**Key words:** stars: abundances – stars: activity – stars: atmospheres – stars: fundamental parameters – stars: individual: RS CVn binaries

## 1. Introduction

With the improved spectral resolution of the X-ray detectors onboard the ASCA and EUVE satellites, it became possible to resolve individual emission lines (or line complexes) of the X-ray spectra from stellar coronae. These highly resolved spectra allowed for the first time the determination of coronal abundances of stars other than the Sun. It was a great surprise that all active stars investigated so far were found to have rather low coronal abundances. For example, in the RS CVn system AR Lac the coronal abundances of O, Mg, Si, S, Ar, Ca and Fe are $3-4$ times lower than the solar photospheric values (White et al. 1994, Singh et al. 1996). Further, in the RS CVn system II Peg the coronal abundances of O, Ne, Mg, Si, S, Ar, Ca, Ni are only $1/2-1/5$ the solar photospheric values, and the Fe abundance is even lower (Mewe et al. 1997). Similarly, in the active single stars $\beta$ Cet and $\pi^1$ UMa the elements N, O, Ne, S, and Fe were found to be underabundant; only Mg appears to be overabundant relative to the solar photospheric values (Drake et al. 1994). As these stars are nearby (mostly within $50\,\mathrm{pc}$) and have low proper motion, their photospheric abundances are expected to be similar to those of the Sun. If true there would be a metallicity gradient across the atmosphere of active stars. On the Sun, there actually is a metallicity gradient across its atmosphere; thereby, the elements N, O, Ne, Ar having a high first ionization potential (FIP) are underabundant (relative to H) in the corona by a factor of $3-4$ compared to the photosphere, while the low-FIP elements Fe, Mg, Si, Ca, Na have the same relative abundances in the photosphere and the corona (Meyer 1985, Feldman & Widing 1990).

The key question of whether there is a metallicity gradient in active stellar atmospheres can be addressed only if accurate coronal and photospheric abundances are available. Meanwhile, coronal abundances have been determined for a number of active stars with ASCA and EUVE, but photospheric abundances are known only for few of them. For the most active stellar coronae, the RS CVn binaries, the photospheric abundance distribution is practically unknown. So far, there are the studies of Fekel & Balachandran (1993) and Randich et al. (1993, 1994), aimed at determining the Li abundances of these systems; thereby, Fe abundances were obtained as byproduct of the analysis, but other metal abundances were not determined. However, neither study performed a purely spectroscopic, self-consistent analysis, and thus the given stellar parameters and abundances are not very reliable. Specifically, Randich et al. (1993, 1994) derived the effective temperature from photometry, resulting in largely uncertain temperature values and Fe abundances. Furthermore, inconsistent results were obtained for the stellar parameters and abundances of systems analyzed in both studies. Specifically, Fekel & Balanchandran (1993) derived approximately solar-like Fe abundances; in contrast, Randich et al. (1993, 1994)

found a significant metal-deficiency, which is hard to explain theoretically due to the close proximity and the low proper motion of the RS CVn systems. As Randich et al. (1993, 1994) also derived different Fe abundances for the two components of several SB2 RS CVn binaries, they noted that "the spectral lines could be significantly affected by surface activity (spots and plages) and may not represent a true metal deficiency".

The present discussion about the coronal abundances of active stars and the existence of an atmospheric metallicity gradient requires the accurate knowledge of the stellar parameters and photospheric abundances. Further, the effect of stellar activity features (spots and plages) on the derived parameters has to be specified. To provide this information is the goal of our study. For this purpose we have selected a sample of active stars, including single stars and SB1 binary systems, which are especially suited for such an analysis. Our spectroscopic study is based on high-resolution, high-SN optical spectra, which cover the entire visible wavelength range and contain all important absorption lines. This broad spectral coverage has two essential advantages for the subsequent analysis: First, we are able to determine all stellar parameters and abundances exclusively from the stellar spectrum. Such a purely spectroscopic analysis is the basis of a self-consistent parameter determination, by which the analysis procedure is iterated until a self-consistent solution is obtained. As the stellar parameters are interdependent on each other, a self-consistent analysis is required to obtain accurate parameters and abundances. Second, we are able to derive different elemental abundances simultaneously. In this paper we concentrate on the abundances of Fe, Mg, and Si, which have similar first ionization potentials (FIPs), but different atomic masses. For each metal, our spectra contain several absorption lines, from which we can calculate a mean metal abundance having a high statistical accuracy. Specifically, our Fe abundance is derived from about 10 Fe II lines, which are much more reliable than the Fe I lines used by the previous studies. To study the influence of stellar activity features on the derived parameters and abundances, we have included some short-period systems in our sample, from which phase-resolved spectra can be taken easily. Due to the inhomogeneous distribution of the activity features on the stellar surface, the activity level of the visible hemisphere will vary with stellar rotation; that may result in a variation of the stellar parameters with rotational phase. Therefore, the influence of stellar activity on the derived parameters and abundances may be detected by our phase-resolved spectroscopy. Finally, we compare the derived photospheric abundances with the coronal abundances recently determined with ASCA and EUVE, and address the key question of whether there is a metallicity gradient in the atmospheres of active stars.

In Sect. 2, we define the selection criteria for our sample stars. Further, we give an overview of the observations and describe the reduction of the raw spectra. Sect. 3 is concerned with the spectral analysis technique. Specifically, we describe the applied model atmospheres and the self-consistent determination of the stellar parameters and metal abundances. The modelling procedure is tested on the solar spectrum. In Sect. 4, we provide the resulting stellar parameters and abundances of our sample stars, and discuss the effect of stellar activity on the derived parameters. In Sect. 5, we compare in detail our parameters to those of previous studies. Finally, we examine possible correlations between the photospheric and coronal abundances and discuss the question of a metallicity gradient.

## 2. Observations and data reduction

### *2.1. The star sample*

To keep the spectral model and the derived stellar parameters as simple and reliable as possible, the sample stars were selected according to the following criteria:

(i) *Single stars and SB1 RSCVn-systems*. Their spectra are described by a one-component model, which is defined by the stellar parameters of one star. A one-component model is the most basic modelling approach and the derived stellar parameters are as certain as the underlying model. For SB2 systems, a two-component model would have to be used; thereby, the relative continuum contribution of the two stars has to be fixed. As this quantity is rather uncertain, the two-component model is not well defined. Therefore, the derived stellar fit parameters are more uncertain, as well.

(ii) *Low to moderate $v \sin i$ values*. The spectra of cool stars contain many absorption lines, which in part are lying closely together. For slowly rotating stars, the rotational line broadening is small and only few lines are rotationally blended. Therefore, we selected mainly slowly rotating stars with $v \sin i < 10$ km/s. For faster rotating stars, the absorption lines are strongly broadened and thus merge with neighbouring lines. The strong line blending makes it difficult to determine the continuum level. For this reason, stars with $v \sin i > 10$ km/s were selected only in order to study the variation of the stellar parameters with rotation.

(iii) *Spectral type G*. First, hotter stars have less absorption lines in their spectra than cooler stars. Specifically, G and very early K stars do not contain too many absorption lines and possess a well-defined continuum level between the lines. The spectra of cooler stars are crowded with lines, arising mainly from the rare earth elements and from molecules, so that the determination of the continuum level is very difficult. Second, hotter stars have a higher contrast between the quiescent photosphere and the star spot. In Table 1, the ratio between the continuum fluxes from spots and quiescent photosphere is calculated for different values of the spot covering fraction. For $\kappa$ Cet, a spot covering fraction of less than $2\%$ was determined by Dorren & Guinan (1994). The other single stars $\beta$ Cet and $\pi^1$ UMa are expected to have spot fractions less than $10\%$, too. For the more active RS CVn systems, the spot fraction is typically between $10-30\%$. For EI Eri, $\lambda$ And and II Peg, spot fractions of $10-20\%$ (Strassmeier 1990, O'Neal et al. 1996), $12\%$ (Donati et al. 1995), and $20-50\%$ (Byrne et al. 1995, O'Neal et al. 1996), respectively, were derived. Table 1 shows that, if the spot fraction is not too large, the spot component contributes little to the total flux at $H_\alpha$ and still less at $H_\beta$. Thus, the spot component can be neglected relative to the flux of the quies-

**Table 1.** Ratio $r_\lambda$ between the continuum fluxes from spots and quiescent photosphere for a fraction $f_s$ of the projected hemisphere covered by spots. The flux ratio is given by $r_\lambda = f_s \cdot B_\lambda(T_s)/(1-f_s) \cdot B_\lambda(T_q)$, with $B_\lambda(T)$ being the radiation of a black body with temperature T.

| Spectral type | $r_{H_\alpha(H_\beta)}(f_s = 0.1)$ | $r_{H_\alpha(H_\beta)}(f_s = 0.3)$ | $r_{H_\alpha(H_\beta)}(f_s = 0.5)$ |
|---|---|---|---|
| G0 ($T_q = 5948K, T_s = 3700K$) | 1% (0.6%) | 4% (2%) | 10% (5%) |
| G5 ($T_q = 5678K, T_s = 3700K$) | 1% (0.7%) | 5% (3%) | 12% (6%) |
| K0 ($T_q = 5273K, T_s = 3500K$) | 1% (0.7%) | 5% (3%) | 12% (6%) |
| K3 ($T_q = 4925K, T_s = 3500K$) | 2% (1%) | 7% (4%) | 16% (9%) |
| K4 ($T_q = 4791K, T_s = 3500K$) | 2% (1%) | 8% (4%) | 18% (10%) |

*Columns*: (1) Spectral type of the star, with $T_q$ and $T_s$ being the temperatures of the quiescent photosphere and the spots, (2)-(4) flux ratio $r_\lambda$ at the wavelengths $\lambda = H_\alpha(H_\beta)$ for a spot fraction $f_s = 0.1, 0.3, 0.5$.

**Table 2.** The star sample containing three active single stars and six RS CVn binaries.

| Name | HD | $V$ | $\Delta V$ | $B-V$ | SpType | $P_{rot}$ (d) | $v \sin i$ (km/s) | Ref. |
|---|---|---|---|---|---|---|---|---|
| $\beta$ Cet | 4128 | 2.04 | | 1.02 | K0III | 80[a] | 3 | Y |
| $\kappa$ Cet | 20630 | 4.83 | | 0.67 | G5V | 9.24 | 8 | D |
| $\pi^1$ UMa | 72905 | 5.60 | | 0.62 | G1.5Vb | 4.69 | 9 | D |
| AY Cet | 7672 | 5.47 | 0.22 | 0.90 | WD/G5III | 77.22 | 6 | S |
| VY Ari | 17433 | 6.9 | 0.1 | 0.96 | G9V | 16.42 | 6 | S |
| EI Eri | 26337 | 6.96 | 0.2 | 0.67 | G5IV | 1.945 | 50 | S |
| IM Peg | 216489 | 5.60 | | | | 24.39 | | S |
| $\lambda$ And | 222107 | 3.7 | 0.28 | 1.01 | G8IV-III | 53.952 | 10 | S |
| II Peg | 224085 | 7.2 | 0.43 | 1.01 | K2V-IV | 6.718 | 21 | S |

*Columns*: (1) Stellar identification, (2) HD number, (3) $V$ magnitude, (4) $\Delta V$ amplitude, (5) $B-V$ color, (6) spectral type, (7) rotational (photometric) period, (8) projected rotational velocity, (9) reference.

*References*: S: Strassmeier et al. (1993); D: Donahue et al. (1996); Y: Young et al. (1989)

cent photosphere, and a one-component model spectrum may be used.

(iv) *SP and LP systems*. The effect of stellar activity (spots and plages) on the derived parameters can be investigated by exploiting the fact that these features are distributed inhomogeneously over the stellar surface and thus the activity level of the visible hemisphere varies with stellar rotation. If the spots and plages actually affect the derived stellar parameters, then the latter should vary with rotation, too. To search for a variation of the derived parameters during the available observing time of three nights (see Sect. 2.2), we had to include some short-period (SP) systems, having rotational periods of less than about 9 d, in our sample. We selected specifically SP systems with a large $\Delta V$ amplitude, for which a variation of the stellar parameters is most likely. The selected SP systems are $\kappa$ Cet, $\pi^1$ UMa, EI Eri, and II Peg. The remaining sample stars are long-period (LP) systems.

The sample stars together with their relevant properties are listed in Table 2.

### *2.2. Observations*

The observations were performed from October 24 to 26, 1996, at the 2.2 m telescope of the Calar Alto observatory in Spain. The spectra were taken with the FOCES echelle spectrograph, which is coupled to the cassegrain focus by fiber optics (Pfeiffer et al. 1998). FOCES provides a spectral coverage between $4000-10000$ Å, taken in one exposure within about 80 orders. The echelle spectra were read out by a $2048^2$ Loral chip, having a pixel size of 15 $\mu$m. The slit width of the spectrograph was set to 100 $\mu$m. With this instrumental set up, the resolution of the FOCES spectra is $R = 65000$.

Table 3 gives an overview of the observations. For the SP systems, spectra were taken every night or every second night to cover different phases of the rotational period, enabling us to study the variability of the derived parameters. For the longer period systems, one spectrum taken in either night is sufficient to derive the stellar parameters; sometimes, a second spectrum was taken in another night to check the reproducibility of the obtained parameters. In addition to the stellar spectra, the solar spectrum reflected from the Moon was observed to obtain the instrumental profile and to test the data reduction and modeling procedures. The exposure times were choosen to provide a S/N

**Table 3.** Log of observations taken with the FOCES echelle spectrograph in October 1996.

| Star | Obs. date (Oct.1996) | Exp. time (s) | S/N |
|---|---|---|---|
| $\beta$ Cet | 24 | 120 | 130 |
| | 26 | 90 | 210 |
| $\kappa$ Cet | 24 | 1000 | 100 |
| | 25 | 1200 | 90 |
| | 26 | 400 | 150 |
| $\pi^1$ UMa | 24 | 1200 | 80 |
| | 26 | 1000 | 130 |
| AY Cet | 24 | 1200 | 90 |
| VY Ari | 24 | 1800 | 70 |
| EI Eri | 25 | 3000 | 50 |
| | 26 | 3000 | 130 |
| IM Peg | 24 | 1800 | 120 |
| $\lambda$ And | 24 | 1200 | 180 |
| | 25 | 1200 | 150 |
| II Peg | 24 | 3600 | 70 |
| | 26 | 2000 | 100 |
| Moon | 25 | 60 | 120 |

ratio of about 100; they mainly reflect the stellar $V$ magnitude, but also the seeing conditions and the instrumental set-up.

### *2.3. Data reduction*

The reduction of the raw spectra was performed with the MIDAS echelle package. We describe here the main steps of the data reduction only briefly and refer to the ESO-MIDAS User Guide, Vol. B (1995) for details.

(i) *Preprocessing*. The bias and flat-field frames are taken as the median of the individual bias and flat-field exposures in order to increase the S/N and to discard bad pixels or particle hits. Similarly, the wavelength calibration and object frames are taken as the mean of the individual wavelength calibration and object exposures in order to increase the S/N. The flat-field, wavelength calibration and object frames then are bias-subtracted and rotated to the standard orientation.

(ii) *Calibration*. The echelle order definition is done on the flat-field frame by applying the Hough-transform method. The wavelength calibration is performed by using the MIDAS thorium-argon line table to compute the dispersion relation, and has an accuracy of a few $10^{-3}$ Å.

(iii) *Reduction*: The inter-order background is calculated by a 2D spline interpolation. The background-subtracted object and flat-field frames are order-extracted. The object frame is divided by the flat-field, wavelength-calibrated and rebinned into $0.05$ Å bins. Merging the $80$ echelle orders yields the 1D object spectrum. The continuum level is defined by polynomial fit through a series of selected line-free points, and normalized to unity.

## 3. Spectral analysis technique

### *3.1. Model atmospheres*

Our determination of the stellar parameters is based on line-blanketed LTE model atmospheres (see Fuhrmann et al. 1997 and references therein). The model atmospheres are calculated with the new opacity line list of Kurucz (1995), which is extended considerably compared to the previous opacity list of Kurucz (1979). After the great debate on the solar Fe abundance during recent years, the meteoritic abundance value with $\log_{10} H = 12.00$ and $\mathrm{Fe} = 7.51$ has come to be preferred in recent studies on this issue. We also adopt the meteoritic value for the Fe abundance in our analysis. For the Mg and Si abundance, we adopt the values $\mathrm{Mg} = 7.53$ and $\mathrm{Si} = 7.50$ from Holweger et al. (1990). We note that the solar abundance mixture, proposed by Anders & Grevesse (1989) with $\log_{10} H = 12.00$, $\mathrm{Mg} = 7.58$, $\mathrm{Si} = 7.55$ and $\mathrm{Fe} = 7.67$, contains a somewhat higher iron abundance.

### *3.2. Self-consistent determination of stellar parameters*

The synthetic spectra from a stellar model atmosphere are determined by four parameters — the effective temperature $T_{eff}$, the surface gravity $\log g$, the metal abundance [M/H][1] and the microturbulence $\xi_t$. Due to the mutual dependence between the parameters, a reliable analysis is rendered impossible if only one parameter is wrong. Specifically the elemental abundances are sensitive to uncertainties in the stellar parameters. Therefore, it is necessary to determine all four stellar parameters in a self-consistent way. This study provides the first self-consistent determination of stellar parameters for our sample stars. The broad spectral bandpass of FOCES together with the line synthesis technique allow us to derive all four stellar parameters purely from the spectrum. To take into account the mutual dependence between the parameters, our analysis procedure is iterated until a self-consistent set of parameters is obtained. In the following, we describe in detail the determination of the individual stellar parameters and metal abundances.

#### 3.2.1. Effective temperature

In most of the previous studies of cool active stars, the metal abundances are derived spectroscopically, while the effective temperature is determined from $B - V$. But photometric temperatures generally are not very reliable because photometry often depends on uncertain calibration procedures and zero points. For active stars, the colors additionally are affected by star spots. As the spots are much cooler than the undisturbed stellar surface, the photometric temperature is significantly lower than the temperature of the undisturbed photosphere, which is required for the abundance determination. For subgiants, the colors are

[1] The metal abundance $[\mathrm{M/H}] \equiv \log[(\mathrm{Fe/H})/(\mathrm{Fe/H})_\odot]$ is usually set equal to the Fe abundance, normalized to the solar photospheric value and given in logarithmic units.

affected by interstellar reddening, which can be accounted for only roughly.

A more direct and more reliable method to determine $T_{eff}$ is by spectroscopy. As the Balmer lines are very sensitive to the temperature, they are well suited to serve as a temperature indicator. For a detailed discussion of the Balmer line method, we refer to Fuhrmann et al. (1993, 1994) and describe here only those aspects which are of special interest for our analysis: (i) $T_{eff}$ is determined from the wings of the Balmer lines, which, in contrast to the line cores, are not sensitive to NLTE-effects. Therefore, also the derived $T_{eff}$ is not affected by NLTE. (ii) As the higher Balmer series members are difficult to analyze, we use only $H_\alpha$ and $H_\beta$ to determine $T_{eff}$. (iii) Using both $H_\alpha$ and $H_\beta$, we are able to derive $T_{eff}$ with an internal[2] accuracy of 70 K. (iv) For the most active sample stars, $H_\alpha$ is strongly filled up with chromospheric emission; then, $T_{eff}$ is determined only from $H_\beta$.

### 3.2.2. Fe abundance and microturbulence

The iron abundance [Fe/H] and the microturbulence are determined simultaneously from an equivalent width (EW)-based analysis of a number of selected iron lines. We provide a list of 129 iron lines in the wavelength range $4900 - 8000$ Å. The free parameters of the line profiles, mainly the line strength and the broadening parameters, are adjusted to the Kitt Peak solar spectrum (see Fuhrmann et al. 1997). The broad spectral bandpass of FOCES allows us to select only the unblended lines of this list, for which the EWs can be measured reliably. It depends on the stellar parameters, mainly on the effective temperature, which lines of the list are unblended.

For each iron line selected, the local continuum level is refined very accurately by a comparison of the stellar spectrum with the Kitt Peak spectrum. Then, the EWs are measured by numerically integrating over the line profile. Stars with $v \sin i > 20$ km/s show a strong rotational broadening, and nearly all their lines are blended. Therefore, the EWs of the very rapdily rotating stars EI Eri, IM Peg and II Peg are determined by the profile synthesis of a 4 Å-wide region around the iron line. For each spectrum, we measure about 10 Fe II and 20 Fe I lines to provide enough data points for an accurate determination of [Fe/H] and $\xi_t$. Only for the very rapidly rotating stars, the analysis is based on fewer lines.

In our EW-based analysis procedure, only EWs between $20-200$ mÅ are used. Smaller EWs can be measured only with a large relative error, larger EWs become insensitive to [Fe/H] and $\xi_t$ and instead are sensitive to $\log g$. The measured EWs are lowered by 1% to take into account the asymmetry in the observed line profile due to turbulent flows. Then, the measured EWs are compared to theoretical EWs, computed for a grid of model atmospheres, according to the following procedure: The model atmosphere parameters $T_{eff}$ and $\log\ g$ are fixed to their values derived from the Balmer line method and the Mg line method (see Sect. 3.2.3). The parameter $\xi_t$ is stepped through a grid of likely $\xi_t$ values. For each $\xi_t$, the parameter [Fe/H] is computed as a function of EW. The correct $\xi_t$ is found from the requirement that the iron abundance is independent of the EW (i.e., the least square fit to the [Fe/H] values as a function of EW has zero slope). This requirement simultaneously determines the iron abundance. The procedure was performed for the Fe I and Fe II lines separately, resulting in two solutions for [Fe/H] and $\xi_t$. We adopt the solution from the Fe II lines because these, in contrast to the Fe I lines, are insensitive to uncertainties in the effective temperature and the temperature stratification and to NLTE-effects. The solution derived from the Fe I lines is used only for comparison. The EW-based iron line analysis allows us to determine [Fe/H] and $\xi_t$ with an internal[2] accuracy of 0.05 dex and 0.1 km/s, respectively.

### 3.2.3. Mg abundance and surface gravity

The magnesium abundance [Mg/H] and the surface gravity are obtained by the line profile synthesis of two Mg lines. This method of determining $\log\ g$, the so-called strong line method, was recently proposed by Fuhrmann et al. (1997). In the first step, [Mg/H] is derived from the analysis of a weak, $\log\ g$-insensitive Mg line. In the second step, $\log\ g$ is determined from the profile synthesis of a very strong Mg line, whose extended wings are sensitive to $\log\ g$. The free parameters of the Mg line profiles are adopted from Fuhrmann et al. (1997). As is emphasized by Fuhrmann et al. (1997), the strong line method is a much more robust and reliable tracer for $\log\ g$ than the ionization equilibrium, which is susceptible to overionization effects and uncertainties in the temperature structure of the model atmosphere.

In the following, we describe the main steps of our Mg line synthesis procedure: (i) Before starting the line synthesis, the stellar model atmosphere, defined by $T_{eff}$, $\log\ g$, [M/H] ($\equiv$ [Fe/H]) and $\xi_t$, has to be specified. $T_{eff}$ is known from the Balmer line method, [Fe/H] and $\xi_t$ from the EW-based iron line analysis. A guess value for $\log\ g$ is obtained from the ionization equilibrium of Fe I and Fe II. (ii) The most suited weak Mg line in the visible range is $\lambda 5711$, because it is practically unblended and quite insensitive to changes in $\log\ g$. The theoretical profiles are convolved with the rotational broadening parameter $v \sin i$, the radial-tangential macroturbulence $\zeta_{RT}$, and the instrumental profile (a Gaussian of 4.4 km/s; see Sect. 3.3). The $\lambda 5711$ profile fit is performed by adjusting the Mg abundance [Mg/H] and the combined broadening parameter $v \sin i + \zeta_{RT}$. The internal[2] accuracy of the derived [Mg/H] value is 0.05 dex. (iii) Once the Mg abundance is fixed, the surface gravity is the only free parameter in fitting the profiles of the strong Mg Ib lines. Due to their extended wings, the Mg Ib lines are highly sensitive

[2] For the spectra presented here, the internal errors of the stellar parameters are determined mainly by the S/N ratio. The given errors hold for the average $S/N$ of about 100. For the higher (lower) quality spectra, the stellar parameters possess a somewhat higher (lower) accuracy than is indicated by the given errors. The systematic (external) errors result from uncertainties in the adopted atomic data, NLTE-effects, the definition of the continuum, and possibly from the effects of stellar activity features (spots and plages). A discussion of the systematic errors is given in Sect. 3.3.

to changes in $\log\ g$. In our analysis, we choose the Mg Ib line at $\lambda 5183$ (having an instrumental profile of $4.6$ km/s; see Sect. 3.3). We note that the left wing of $\lambda 5183$ is affected by small MgH-lines, so that only the right wing is used for adjusting $\log\ g$. The internal[2] accuracy, with which the $\log\ g$ value can be derived, amounts to $0.1$ dex.

#### 3.2.4. Si abundance

Analogously to the Mg abundance, the Si abundance [Si/H] is determined from the line profile analysis of several weak Si lines. Grupp (1997, priv. comm.) kindly provided a list of nine Si lines in the range of $5600 - 6800$ Å, whose atomic data were adjusted to the Sun. This list contains seven Si I and two Si II lines. As the Si II lines are much more robust with respect to temperature uncertainties and NLTE-effects, they are used preferrentially in the analysis. As in the Mg line synthesis, the theoretical profile is convolved with the broadening parameters $v \sin i$ and $\zeta_{RT}$ and with the instrumental profile (see Sect. 3.3); then, the Si line profile is fitted by adjusting [Si/H]. The Si lines, which we select from the list for determining the Si abundance, depend on the atmospheric parameters and the rotational broadening of a specific star. We use only lines which are nearly unblended and have a well defined continuum level. With this criterion, typically $2 - 4$ Si lines per stellar spectrum can be used. The thus derived [Si/H] values are expected to be very reliable. As the final Si abundance is taken as the mean of the individual [Si/H] values, it has a much smaller statistical error than the individual [Si/H] values. Specifically, the internal[2] accuracy of the final [Si/H] value amounts to $0.05$ dex.

### *3.3. Application to the solar spectrum*

The above described reduction and analysis procedures are tested on the solar spectrum. On October 25, 1996, we obtained a $1$ min exposure of the solar spectrum (reflected moon light) with $S/N \simeq 120$ (see Table 3). Applying our reduction and analysis procedures to the solar spectrum yields the following self-consistent set of parameters: The effective temperature, derived from the $H_\alpha$ and $H_\beta$ profiles, amounts to $T_{eff} = 5780$ K. The Fe abundance and microturbulence, determined from the EW-based analysis of 10 Fe II lines, yields $[\mathrm{Fe/H}] = +0.04$ dex and $\xi_t = 0.82$. The surface gravity and the Mg abundance, derived with the strong line method, amount to $\log g = 4.41$ and $[\mathrm{Mg/H}] = +0.02$ dex. For comparison, the solar atmospheric parameters given by the literature (e.g., Gray 1992) are $T_{eff} = 5780 \pm 20$ K, $\log g = 4.44$, $\xi_t = 1.0$, $[\mathrm{Fe/H}] = 0.0$ dex, and $[\mathrm{Mg/H}] = 0.0$ dex. Obviously, the published values for the solar $T_{eff}$, $\log g$, [Fe/H], and [Mg/H] are within the internal error ranges of our derived parameters. Only the published solar $\xi_t$ differs from our $\xi_t$ by about twice the internal error. The good agreement of our parameters with the published solar values confirms the finding of Fuhrmann et al. (1995) that the systematic[2] (external) errors caused by uncertainties in the adopted atomic data, NLTE-effects, and the definition of the continuum largely cancel, because the applied analysis method is differential to the Sun. The comparison with the published solar values shows that the systematic errors (except possible effects of stellar activity) have at most the same magnitude as the internal errors. Possible effects of stellar activity on the derived parameters are investigated in detail in Sect. 4.2. Thus, our reduction and analysis procedure is able to reproduce the solar parameters with high accuracy.

The second reason for observing the solar spectrum is to obtain the instrumental profile of the FOCES spectrograph equipped with the $2048^2$ Loral chip. For this purpose, the FOCES spectrum of the Sun having a resolution of $65000$ is compared with the Kitt Peak spectrum having approximately an infinite spectral resolution. Convolving the Kitt Peak spectrum with a finite resolving power and fitting it to the FOCES solar spectrum yields the unknown instrumental profile of FOCES equipped with the $2048^2$ chip. For $\lambda < 5500$ Å, the instrumental profile slightly variies with wavelength; it amounts to $5.0$ km/s at $\lambda \simeq 4800$ Åand decreases to $4.2$ km/s at $\lambda \simeq 5800$ Å. For $\lambda > 5800$ Å, the profile is nearly constant at about $4.2$ km/s. The variation of the FOCES profile at shorter wavelengths is caused probably by the fact that the performance of the chip is worse towards its edges where the blue part of the spectrum is located.

## 4. Results

### *4.1. Stellar parameters and metal abundances*

The stellar parameters derived for our sample stars are listed in Table 4. Each line of the table represents a self-consistent set of parameters. The first two columns give the star's name and the date of the observation. For the SP systems $\kappa$ Cet, $\pi^1$ UMa, EI Eri and II Peg, spectra from different nights are analyzed to detect a possible variation of the stellar parameters with rotation. Also for some LP systems, spectra from different nights are analyzed to enable a comparison between statistical and true variations of the stellar parameters. As each star was observed at about the same time during the night, the observations from subsequent nights differ in time by about $24$ h and in phase by about $1/P_{rot}[d]$. The third column contains the rotational phase at the time of the observation relative to the first observation of the star.

The effective temperature, listed in column 4, is derived for the individual stars as follows: (i) For $\beta$ Cet, $\kappa$ Cet, $\pi^1$ UMa, AY Cet and $\lambda$ And, both $H_\alpha$ and $H_\beta$ are suited to perform the profile synthesis. For all these stars, except AY Cet, the $T_{eff}$ values derived from the two lines agree very well. For AY Cet, the $T_{eff}$ value from $H_\alpha$ is lower by about $200$ K than that from $H_\beta$. This probably indicates the existence of large spots on the surface of AY Cet, which affect the spectrum at $H_\alpha$ more than at $H_\beta$ (see Table 1). Assuming this scenario, $H_\beta$ is the more reliable temperature indicator, and we derive $T_{eff}$ only from this line. (ii) For IM Peg, only $H_\alpha$ is suited for the profile synthesis, because the $H_\beta$ profile is disturbed significantly by broad molecular lines as a result of the low temperature and fast rotation of the star. (iii) VY Ari, EI Eri and II Peg are so active

**Table 4.** Stellar parameters of the sample stars.

| Star | Date (in Oct, 1996) | Φ | $T_{eff}$ (K) | $\log g$ | $\xi_t$ | [Fe/H] | [Mg/H] | [Si/H] | $v \sin i + \zeta_{RT}$ (km/s) |
|---|---|---|---|---|---|---|---|---|---|
| $\beta$ Cet | 24 | | 4800 | 2.8 | 1.65 | 0.06 | -0.01 | 0.27 | 2.5+5.0 |
| | 26 | | 4800 | 2.7 | 1.50 | 0.05 | 0.05 | 0.34 | 3.0+5.0 |
| $\kappa$ Cet | 24 | 0 | 5660 | 4.35 | 1.37 | -0.01 | -0.02 | 0.03 | 3.6+4.1 |
| | 25 | 0.11 | 5700 | 4.40 | 1.44 | 0.01 | 0.04 | 0.08 | 4.2+4.8 |
| | 26 | 0.22 | 5680 | 4.42 | 1.31 | -0.06 | -0.01 | 0.05 | 4.5+4.1 |
| $\pi^1$ UMa | 24 | 0 | 5820 | 4.38 | 1.29 | 0.00 | -0.03 | 0.10 | 9.0+4.2 |
| | 26 | 0.43 | 5840 | 4.47 | 1.26 | -0.09 | -0.14 | -0.06 | 9.2+4.1 |
| AY Cet | 24 | | 5080 | 3.0 | 1.7 | -0.38 | -0.22 | -0.31 | 4.5+4.5 |
| VY Ari | 24 | | 4800 | 3.1 | 1.5 | -0.09 | 0.02 | -0.03 | 10.0+4.5 |
| EI Eri | 25 | 0 | 5620 | 3.55[a] | 1.06 | -0.03 | -0.08 | -0.04 | 53.0+3.5 |
| | 26 | 0.51 | 5620 | 3.55 | 0.95 | 0.03 | 0.01 | -0.03 | 53.0+3.5 |
| IM Peg | 24 | | 4800 | 2.9 | 1.40 | -0.11 | 0.02 | 0.00 | 24.0+4.5 |
| $\lambda$ And | 24 | | 4800 | 3.0 | 1.70 | -0.40 | -0.22 | -0.26 | 6.0+4.5 |
| | 25 | | 4800 | 3.0 | 1.40 | -0.37 | -0.15 | -0.27 | 6.0+4.5 |
| II Peg | 24 | 0 | 4800 | 3.65 | 1.40 | -0.24 | -0.14 | -0.15 | 20.0+4.5 |
| | 26 | 0.30 | 4800 | 3.65 | 1.44 | -0.19 | -0.15 | -0.09 | 20.0+4.5 |

*Columns*: (1) Stellar identification, (2) date of observation, (3) rotational phase (relative to the first observation), given only for the SP systems, (4) effective temperature, (5) surface gravity, (6) microturbulence, (7)-(9) Fe, Mg, Si abundances relative to the solar photospheric values in logarithmic units (see Sect. 3.2), (10) sum of projected rotational velocity and macroturbulence.

*Notes*: a: As the spectrum of Oct. 26 has a much better quality than that of Oct. 25, and the gravity is independent from rotational phase, we adopted the $\log g$ value of Oct. 26.

that $H_\alpha$ is filled in strongly with chromospheric emission, or even is completely in emission. In this case, the temperature is derived only from $H_\beta$. II Peg was even so active that $H_\beta$ also has a strong central emission peak; therefore, only the outermost line wings are used for the profile fit. We note that the uncertainty in $T_{eff}$, given as 70 K (see Sect. 3.2.1), represents a mean value for our sample stars. Actually, the $T_{eff}$ accuracy amounts to about 50 K for $T_{eff} > 5000$ K and about 100 K below.

The surface gravity obtained from the Mg Ib line is given in column 5. Similar to the lower accuracy of the Balmer line method for low temperatures, the accuracy of the Mg Ib line method decreases somewhat for low gravities. This means that the $\log\ g$ values of the dwarfs $\kappa$ Cet and $\pi^1$ UMa and the slightly evolved stars EI Eri and II Peg have a higher accuracy than those of the more evolved sample stars. In column 6, the microturbulence obtained from the EW-based iron line analysis is listed. The $\xi_t$ values of our sample stars within their error ranges confirm the $\xi_t$ characteristic derived by Fuhrmann (1997, priv. comm.) for a large stellar sample: For main sequence stars, $\xi_t$ increases with effective temperature; for a fixed temperature, $\xi_t$ increases with decreasing surface gravity.

The Fe, Mg and Si abundances relative to their solar photospheric values are given in columns $7-9$. The Fe abundance is determined from the EW-based iron line analysis, the Mg and Si abundances are obtained from individual line profile synthesis. The abundances are very accurate for the slowly rotating sample stars with $v \sin i < 20$ km/s. For the few faster rotating sample stars, the abundances may be somewhat less accurate due to the unavoidable line blending. Finally, the projected rotational velocity and the macroturbulence are listed in column 10. We note that only the sum of the two broadening parameters can be determined precisely, as $v \sin i$ and $\zeta_{RT}$ have a similar influence on the line profile.

### *4.2. Effect of stellar activity on the derived parameters*

Our sample stars possess very active stellar atmospheres with a dense network of chromospheric plages and a large covering fraction of photospheric spots. The line emission from the plages may fill up the photospheric absorption lines, thus apparently reducing the derived elemental abundances. The flux from the photospheric spots may contribute significantly to the total flux, specifically at the redder part of the spectrum (see Table 1); therefore, the derived effective temperature will be lower than that of the undisturbed photosphere, resulting also in an underestimation of the elemental abundances. Thus, both the chromospheric and photospheric activity features may result in an apparent reduction of the derived effective temperature and elemental abundances.

The effects of stellar activity on the derived parameters will show up only if the activity level and thus the parameters undergo any variation. There are two ways the activity level may vary: First, the stellar rotation causes the inhomogeneously distributed plages and spots to move on and off the visible hemi-

sphere of the star. This mechanism is known as rotational modulation and results in an apparent variation of the activity level with rotational phase. If the stellar parameters are affected by the activity features, then they should vary with rotational phase, too. During the three observing nights available, a variation of the stellar parameters may occur only for the SP systems $\kappa$ Cet, $\pi^1$ UMa, EI Eri and II Peg. Second, the spot area and the plages regions may vary intrinsically by the spontaneous generation or reconnection of magnetic flux. As spots and plages are stable on the timescale of weeks typically, intrinsic variations of the activity level, which would affect both the SP and LP systems, are not very likely during the three day observing interval.

Amongst the LP systems, $\beta$ Cet and $\lambda$ And were observed in different nights (see Table 4). For $\beta$ Cet, the stellar parameters derived from the spectra of Oct, 24 and 26 agree very well within the errors. Similarly, the spectra of $\lambda$ And from Oct, 24 and 25 yield essentially the same parameters within the error ranges, only the $\xi_t$ values have a somewhat larger difference. Thus, the stellar parameters of the LP systems do not show any significant variation during the time of the observations. This result indicates that the stellar activity level does not undergo strong intrinsic variations.

All our SP sample stars, namely $\kappa$ Cet, $\pi^1$ UMa, EI Eri and II Peg, were observed in two or three different nights (Table 4). Thus, spectra from different phases of the rotational period are available, which allow us to study whether the stellar parameters vary with rotational phase. For $\kappa$ Cet, three spectra covering about one fourth of the rotational period are available. The derived parameters do not show any variation with rotational phase; this indicates that the stellar activity does not affect the derived parameters or that the activity level does not vary significantly during the observations. For $\pi^1$ UMa, two spectra were taken from opposite stellar hemispheres. The derived $T_{eff}$, $\log g$, $\xi_t$ and [Fe/H] values are in good agreement, but the [Mg/H] and [Si/H] values are inconsistent with each other. Both metal abundances appear to be higher for the Oct, 24 spectra compared to the Oct, 26 spectra. Interestingly, also the Fe abundance seems to be higher on Oct, 24 than on Oct, 26, although the difference is not significant. Also for EI Eri, two spectra were taken from opposite stellar hemispheres. However, the derived parameters do not vary with rotational period. For II Peg, two spectra covering about one third of the rotational period are available. Again, there is no significant variation of the stellar parameters. Thus, amongst the four systems for which phase-resolved spectra are available, only one system ($\pi^1$ UMa) shows a significant variation of some stellar parameters ([Mg/H] and [Si/H]) with rotational phase. This indicates that stellar activity actually may affect the derived parameters, especially the metal abundances. However, as the variation of the Mg and Si abundances with stellar rotation is not much larger than the corresponding statistical errors, we consider it unlikely that stellar activity causes unrealistically low values of the metal abundances.

## 5. Discussion

### *5.1. Comparison of our parameters with previous studies*

#### 5.1.1. Single stars

The single stars of our sample, $\kappa$ Cet, $\pi^1$ UMa and $\beta$ Cet, are nearby and therefore are spectroscopically well-studied objects. Nevertheless, the previous studies do not provide a sophisticated determination of the stellar parameters and metal abundances comparable to our study for the following reasons: (i) A purely spectroscopic, self-consistent determination of $T_{eff}$, $\log g$ and [Fe/H] (see Sect. 3.2), though not of other metals, was provided so far only for $\kappa$ Cet. In contrast, the previous studies on $\beta$ Cet and $\pi^1$ UMa did not yield a self-consistent set of parameters. Generally, $T_{eff}$ was derived from photometry, $\log g$ from physical parameters, [Fe/H] from spectroscopy, and $\xi_t$ simply was fixed at a guess value. (ii) Another important point is the ion species from which the Fe abundance is derived (see Sect. 3.2.2). While [Fe/H] was determined from the reliable Fe II lines for $\kappa$ Cet and $\beta$ Cet, it was obtained from the less robust Fe I lines for $\pi^1$ UMa. (iii) So far, the surface gravities of $\kappa$ Cet, $\beta$ Cet and $\pi^1$ UMa were determined only from the ionization equilibrium. But Fuhrmann et al. (1997) note that the strong line method (see Sect. 3.2.3) typically yields a higher $\log g$ and a higher [Fe/H] than the ionization equilibrium, which may be distorted by temperature uncertainties and NLTE-effects affecting the Fe I lines. As the line parameters usually are adjusted to the solar spectrum, the $\log g$ and [Fe/H] values derived by the two methods should not differ for solar-like stars, but may do for others. Therefore, we expect to confirm the published $\log g$ and [Fe/H] values of the solar-like stars $\kappa$ Cet and $\pi^1$ UMa, but probably not those of the evolved star $\beta$ Cet.

In the following, we provide a detailed comparison between our results and those of the previous studies for the individual single stars:

*$\kappa$ Cet:* Cayrel de Strobel & Bentolila (1989) determined $T_{eff} = 5630$ K from $H_\alpha$, $\log g = 4.5$ from the ionization equilibrium, and $[\mathrm{Fe/H}] = 0.00(+0.04)$ from the EWs of 1 Fe II (30 Fe I) lines using a curve of growth technique; $\xi_t$ was fixed at 1.0. A comparison with our results shows that all parameters essentially agree very well within their errors. Small differences may result from the different methods applied: First, our $T_{eff}$ value derived from both $H_\alpha$ and $H_\beta$ is slightly higher than their $T_{eff}$ derived from $H_\alpha$ alone, probably because $H_\beta$ is less affected by spots. The higher $T_{eff}$ is supported by Blackwell & Lynas-Gray (1994), who determined $T_{eff} = 5732$ K using the infrared flux method. Second, our $\log g$ value derived from the Mg line is slightly lower than that determined from the ionization equilibrium. Third, our Fe abundance derived from about 10 Fe II lines, is somewhat lower than that determined from Fe I EWs by Cayrel de Strobel & Bentolila (1989); this may depend on temperature uncertainties and NLTE-effects affecting the Fe I lines, and on their $\xi_t$ value fixed somewhat too low.

*$\pi^1$ UMa:* From the three previous studies on $\pi^1$ UMa, only Hearnshaw (1974) provided a complete set of parameters. In that study, $[\mathrm{Fe/H}] = -0.27$ was determined from Fe I EWs

by a curves of growth, while $T_{eff} = 5790$ K was derived from color, $\log g = 4.40$ from parallax, and $\xi_t = 1.3$ was fixed. The two other studies only gave incomplete parameter sets: Boesgaard et al. (1988) determined $T_{eff} = 5850$ K from color, and $[\mathrm{Fe/H}] = -0.08$ from Fe I. Cayrel (1988) adopted the temperature from Boesgaard et al. (1988), and derived an abundance of $[\mathrm{Fe/H}] = -0.01$. Evidently, the three parameter sets are not consistent with each other. Our results support the higher temperature and Fe abundance of Boesgaard et al. (1988) and Cayrel (1988). The very low Fe abundance of Hearnshaw (1974) is expected to result mainy from the too low temperature and/or systematic errors. Our spectroscopic gravity agrees well with that of Hearnshaw (1974) derived from parallax.

*$\beta$ Cet:* Luck & Challenger (1995) derived $T_{eff} = 4750$ K from color, and assumed $\xi_t = 2.4$. They obtained $\log g = 2.45$ from ionization equilibrium, $[\mathrm{Fe/H}] = 0.13 \pm 0.27\,(0.14 \pm 0.12)$ from Fe I (Fe II) and $[\mathrm{Si/H}] = 0.33 \pm 0.18\,(0.80 \pm 0.01)$ from Si I (Si II). However, their physical gravity $\log g = 2.65$ calculated from mass and radius is significantly higher than the spectroscopic one, and yields different abundances $[\mathrm{Fe/H}] = 0.15 \pm 0.27\,(0.26 \pm 0.12)$ from Fe I (Fe II) and $[\mathrm{Si/H}] = 0.38 \pm 0.18\,(0.84 \pm 0.00)$ from Si I (Si II). Gratton & Ortolani (1986) obtained $T_{eff} = 4860$ K from color, $\log g = 2.80$ from ionization equilibrium, $[\mathrm{Fe/H}] = 0.04$, and a best-fit $\xi_t = 1.6$. Finally, Kovacs (1983) derived $T_{eff} = 4800 \pm 50$ K from color, $\log g = 2.5 \pm 0.4$ from ionization equilibrium, $[\mathrm{Fe/H}] = -0.11 \pm 0.22$ from both Fe I and Fe II, and $[\mathrm{Si/H}] = 0.05 \pm 0.27$ from Si I, assuming $\xi_t = 2.3$. A comparison of the three studies shows that their photometric temperatures are consistent with each other, and also agree with our spectroscopic temperature. But, the published $\log g$ values have large associated errors, and therefore show a significant scatter. Our $\log g$ from the Mg Ib line agrees well with the physical gravity and with the value of Gratton & Ortolani (1986), while the other two values from the ionization equilibrium are significantly lower. Similarly, the Fe and Si abundances of the three studies differ largely from one another. Mostly, our spectroscopic abundances are well within their error ranges. Specifically, we confirm the surprisingly high Si abundance by Luck & Challenger (1995).

#### 5.1.2. RS CVn binaries

Compared to our single stars, the RS CVn binaries are not at all spectroscopically well-studied, and their effective temperature, surface gravity, and elemental abundances are very poorly known. Up to now, there are essentially the studies of Fekel & Balachandran (1993) and Randich et al. (1993, 1994), which provided stellar parameters for samples of RS CVn binaries. The two studies applied different analysis methods, and, surprisingly, resulted in significantly different stellar parameters: Fekel & Balachandran (1993) generated a model spectrum of the $6702 - 6712$ Å region, using a giant model atmosphere with first-order stellar parameters. Then, $T_{eff}$ and [Fe/H] were refined by fitting the temperature-sensitive Fe I lines at 6703, 6705, and 6710 Å. Randich et al. (1993, 1994) estimated $T_{eff}$ from $B-V$ with a large error of 250 K, and adopted $\log g$ from spectral type and luminosity class. The microturbulence was fixed at 1 km/s for main-sequence stars, and 1.7 km/s for subgiants and giants. Then, [Fe/H] was determined by fitting the Fe I line at 6704 Å. A comparison between the two studies shows that for five RS CVn binaries common in the two samples significantly different stellar parameters were obtained: Fekel & Balachandran (1993) generally derived higher $T_{eff}$ values than Randich et al. (1993, 1994), with the differences amounting to up to 300 K. Further, extremely different $\log g$ values were provided for 4 (out of 5) stars, with the most extreme example being V1762 Cyg with $\Delta \log g = 1.35$ dex. The two studies also derived significantly different Fe abundances: Randich et al. (1993, 1994) obtained very low abundances with $[\mathrm{Fe/H}] = -0.6$ to $-0.3$, indicating the RS CVn binaries to be unexpectedly metal-poor objects. In contrast, Fekel & Balachandran (1993) derived abundances around the solar photospheric values with $[\mathrm{Fe/H}] = -0.20$ to 0.10. The difference is most extreme for AY Cet and V1762 Cyg, amounting to $\Delta[\mathrm{Fe/H}] = 0.5$ dex.

In this confusing situation, our study will help to solve the puzzle about the photospheric abundances of the RS CVn binaries by applying a substantially improved analysis method for deriving the stellar parameters compared to the previous studies: (i) The Balmer line method applied here, which takes into account both $H_\alpha$ and $H_\beta$, is the most reliable technique to determine the effective temperature. In contrast, the temperatures derived by Randich et al. (1993, 1994) from $B-V$ photometry are highly uncertain, because $B-V$ may be affected strongly by stellar activity features, and, in addition, the calibration procedures required for the convertion of $B-V$ into $T_{eff}$ may be quite inaccurate. Although the Fe I line method of Fekel & Balachandran (1993) provides a more reliable temperature diagnostic, it may suffer from the sensitivity of the Fe I lines towards uncertainties in the temperature stratification and NLTE-effects, and from stellar activity features affecting particularly the red wavelengths. (ii) In neither of the previous studies, the gravity was derived spectroscopically, not even by means of the ionization equilibrium. Thus, the $\log g$ value we derived with the strong line method is the first reliable gravity available for the RS CVn binaries. (iii) Previously, the Fe abundance was determined only from Fe I lines, which are strongly affected by temperature uncertainties and NLTE-effects. Thereby, Fekel & Balachandran (1993) took into account three Fe I lines, Randich et al. (1993, 1994) considered only one line. In our study, the Fe abundance is determined from the very reliable Fe II lines; taking into account about 10 of these lines, we are able to derive [Fe/H] with the required high statistical accuracy. (iv) The present study represents the first effort to derive the stellar parameters of the RS CVn binaries in a self-consistent way. In contrast, the previous studies determined only some of the set of stellar parameters, while fixing the others somehow. Due to the interdependence of the parameters, even the properly derived parameters actually have larger uncertainties than their statistical errors. For example, even if Fekel & Balachandran (1993) determined formally a rather reliable temperature and Fe abundance, these parameters actually are affected by the large

uncertainties of the other parameters. (v) Both previous studies aimed at deriving the Li abundances of RS CVn binaries, and obtained the Fe abundances only as a by-product of their analysis. Other metal abundances, which are of great interest in stellar coronal physics, were not provided by these studies.

In the following, we compare our results with those of the previous studies for the individual RS CVn binaries:

*AY Cet:* With the methods described above, Fekel & Balachandran (1993) obtained $T_{eff} = 5300$ K, $\log g = 3.0$, and $[\mathrm{Fe/H}] = 0.0$, while Randich et al. (1993, 1994) derived substantially lower values for the temperature and Fe abundance of $T_{eff} = 5000$ K and $[\mathrm{Fe/H}] = -0.5$, using $\log g = 3.1$. Further, McWilliam (1990) determined $T_{eff} = 5030$ K from color, a physical gravity $\log g = 3.0$ from $T_{eff}$, luminosity, and mass, and $[\mathrm{Fe/H}] = -0.49 \pm 0.07$ from an EW-based LTE-analysis, assuming $\xi_t = 2.0$. Our stellar parameters are closer to those of Mc William (1990) and Randich et al. (1993, 1994) than to those of Fekel & Balachandran (1993), although we find AY Cet to be less cool and metal-poor than the former authors. AY Cet is the only star within our sample, for which $T_{eff}$ from $H_\alpha$ is significantly lower than that from $H_\beta$, indicating large star spots (see Sect. 4.1). Therefore, $T_{eff} \simeq 5000$ K, as derived from $B-V$, and hence $[\mathrm{Fe/H}] \simeq -0.5$ are probably too low. Nevertheless, AY Cet indeed seems to be metal-deficient, because the abundances of Mg and Si are as low as that of Fe.

*EI Eri:* Fekel & Balachandran (1993) determined $T_{eff} = 5600$ K, $\log g = 3.0$, and $[\mathrm{Fe/H}] = -0.05$. In contrast, Randich et al. (1993, 1994) derived $T_{eff} = 5700$ K, $\log g = 4.1$, and $[\mathrm{Fe/H}] = -0.3$. Finally, O'Neal et al. (1996) adopted a physical gravity of $\log g = 3.8$ and a temperature of the quiescent photosphere of $T_Q = 5600$ K in their analysis of the TiO bands; they found that the spot covering fraction varies from 16 to 37% between three different epochs. Our effective temperature of $T_{eff} = 5620$ K is consistent with the temperature of the quiescent photosphere derived by O'Neal et al. (1996); this indicates that our spectroscopic temperature determination is not affected even by the presence of moderate star spots. Our surface gravity is close to the physical gravity calculated by O'Neal et al. (1996). Furthermore, our temperature and Fe abundance agree well with those of Fekel & Balachandran (1993). The most important result is that the Fe, Mg and Si abundances all are found to be solar-like. Thus, EI Eri definitely is not metal-deficient as was derived by Randich et al. (1993, 1994).

*IM Peg:* So far, the stellar parameters were determined only by Fekel & Balachandran (1993), who found $T_{eff} = 4800$ K, $\log g = 3.0$, and $[\mathrm{Fe/H}] = 0.00$. Their parameters agree well with our results within the error ranges. The Mg and Si abundances, which we derive for the first time, are close to the solar values. The spot covering fraction of IM Peg amounts to $20 - 35\%$ at the time of maximum activity in 1992 September, with the exact value depending on the adopted spot temperature (Dempsey et al. 1996). With an activity cycle of 15 y (Dempsey et al. 1996 and references therein), IM Peg has an intermediate activity level at the epoch of our observations. Nevertheless, IM Peg is found to have solar-like metal abundances. As in the case of EI Eri, we conclude that a moderate activity level does not affect the derived parameters significantly, and, specifically, does not result necessarily in sub-solar abundances.

*$\lambda$ And:* Although Fekel & Balachandran (1993) and Randich et al. (1993, 1994) obtained consistent temperatures of $T_{eff} = 4900$ K and 4850 K, respectively, they derived largely different gravities of $\log g = 3.75$ and 2.8, respectively. Moreover, Fekel & Balachandran (1993) found $\lambda$ And to be only slightly metal-deficient with $[\mathrm{Fe/H}] = -0.2$, while Randich et al. (1993, 1994) derived $[\mathrm{Fe/H}] = -0.6$, indicating the system to be heavily metal-depleted. A comparison between the previous studies and our results shows that our temperature is consistent with the published values. Our gravity of $\log g = 3.0$ and Fe abundance of $[\mathrm{Fe/H}] \simeq -0.4$ are just in between the inconsistent results of the previous studies. Besides Fe, also Mg and Si are found to be underabundant with respect to the Sun; this indicates that $\lambda$ And has probably a true metal-deficiency. However, as the abundance of Fe is lower than that of Mg and Si, the overall metal abundance [m/H] should be larger than $-0.4$. Thus, $\lambda$ And definitely is not as metal-poor as derived by Randich et al. (1993, 1994).

*II Peg:* II Peg was not investigated by Fekel & Balachandran (1993), but is contained in the sample of Randich et al. (1993, 1994). The latter authors determined $T_{eff} = 5050$ K, $\log g = 3.7$, and an unexpectedly low Fe abundance of $[\mathrm{Fe/H}] = -0.5$, indicating II Peg to be metal-poor. Finally, O'Neal et al. (1996) derived a significantly lower temperature of $T_{eff} = 4800$ K from the analysis of the TiO bands, and adopted a physical gravity of $\log g = 3.7$. Our temperature of $T_{eff} = 4800$ K is in excellent agreement with that of O'Neal et al. (1996), and our gravity of $\log g = 3.65$ agrees well with the published values. But, we obtain a significantly higher Fe abundance of $[\mathrm{Fe/H}] \simeq -0.2$ than Randich et al. (1993, 1994). As the Mg and Si abundances of $[\mathrm{Mg/H}], [\mathrm{Si/H}] \simeq -0.15$ are even higher than the Fe abundance, there is evidence that II Peg is only slightly metal-deficient. The spot covering fraction of II Peg was found to be rather large at various epochs of the $8 - 10$ y lasting activity cycle: O'Neal et al. (1996) found $f_S = 40 - 55\%$ in 1989 October and 1992 September, and Byrne et al. (1995) derived $f_S > 30\%$ in 1991. As in the case of EI Eri and IM Peg, we conclude that the effect of stellar activity on the derived parameters, specifically the metal abundances, is not too large even for a remarkably spotted star as II Peg.

*VY Ari:* There is no previous determination of the stellar parameters of VY Ari.

### *5.2. The question of a metallicity gradient in the atmospheres of active stars*

So far, coronal abundances are available for the following sample stars: For $\beta$ Cet, the coronal abundances were determined from X-ray spectra obtained by ASCA (Drake et al. 1994). Specifically, the Fe, Mg, and Si abundances amount to $[\mathrm{Fe/H}] = -0.11$, $[\mathrm{Mg/H}] = 0.16$, and $[\mathrm{Si/H}] = 0.01$. For $\pi^1$ UMa, the coronal abundances were derived also from ASCA spectra, and the abundances are $[\mathrm{Fe/H}] = -0.39$, $[\mathrm{Mg/H}] = 0.05$, and $[\mathrm{Si/H}] = -0.33$ (Drake et al. 1994).

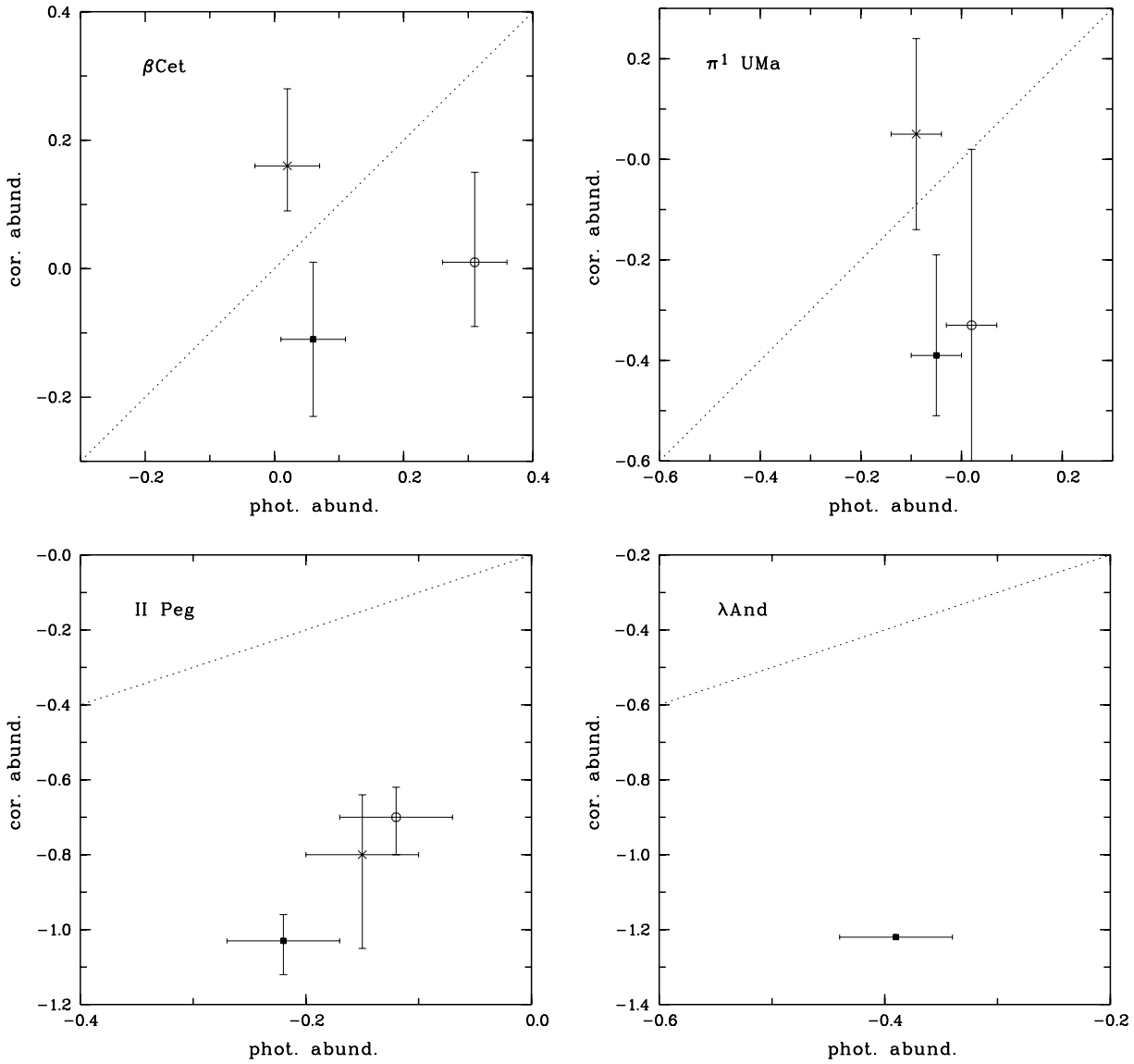


**Fig. 1.** Correlation between the photospheric and coronal Fe (*filled squares*), Mg (*crosses*), and Si (*circles*) abundances for the single stars $\beta$ Cet and $\pi^1$ UMa, and for the RS CVn systems II Peg and $\lambda$ And. The abundance values are given in logarithmic units relative to the solar photospheric values (see Sect. 3.2). The dotted line represents equal coronal and photospheric abundances. Data points below (above) this line indicate an under(over)-abundance of metals in the corona relative to the photosphere.

For II Peg, X-ray spectra from both ASCA and EUVE are available; the derived metal abundances, e.g., $[\mathrm{Fe/H}] = -1.02$, $[\mathrm{Mg/H}] = -0.80$, and $[\mathrm{Si/H}] = -0.70$, are all very low (Mewe et al. 1997). For $\lambda$ And, the coronal Fe abundance was estimated from ROSAT/PSPC spectra as $[\mathrm{Fe/H}] = -1.22$ (Bauer & Bregman 1996). For other sample stars, high-resolution X-ray spectra from ASCA and EUVE are already available, and the coronal abundances will be published soon. Specifically, long-duration ASCA pointings, which have a sufficiently high S/N ratio to allow a careful abundance analysis, are available for $\kappa$ Cet and $\lambda$ And. Further, AY Cet, VY Ari, and $\lambda$ And were identified as EUVE sources. Only for EI Eri and IM Peg are ASCA and EUVE observations still lacking.

Similarly low coronal abundances were found for all other active stars, from which high-resolution X-ray spectra are available (see Sect. 1). However, we explicitely mention that it is not clear yet whether this apparent metal-deficiency is actually true or whether it is an artefact arising from uncertainties in the atomic data (e.g., unresolved lines in the Fe L complex at 1 keV) or from resonant scattering processes (Schrijver et al. 1995). In the following, we discuss the metallicity stratification in the atmospheres of our sample stars and the important question of an atmospheric metallicity gradient on the basis of the published coronal abundances (i.e., on the assumption of a true metal-depletion in active stellar coronae).

In Fig. 1, a comparison between the photospheric and coronal metal abundances is shown for those sample stars for which

coronal abundances are available. The photospheric abundances are taken from Table 4, the coronal abundances together with their $1\sigma$-errors are adopted from the references given above. We note that the comparatively large errors of the coronal abundances are caused mainly by the low S/N-ratio and the low spectral resolution of the X-ray spectra. For the single star $\beta$ Cet, the Fe and Si abundances are significantly underabundant in the corona relative to the photosphere; in contrast, the Mg abundance is significantly overabundant in the corona compared to the photosphere. For the single star $\pi^1$ UMa, the correlation between the photospheric and the coronal abundances is similar to that of $\beta$ Cet, although less significant due to the larger errors in the coronal abundances. Interestingly, the high coronal Mg abundance of $\beta$ Cet and $\pi^1$ UMa is not caused by a correspondingly high photospheric Mg abundance. For the RS CVn system II Peg, all three metal abundances are strongly underabundant in the corona relative to the photosphere. Finally, for the RS CVn system $\lambda$ And, the Fe abundance is strongly depleted in the corona compared to the photosphere.

For all our sample stars, the photospheric Fe, Mg, and Si abundances are concentrated typically within a narrow range. This indicates that the stars, although being slightly metal-depleted, have the same relative distribution of metals as the Sun. The coronal metal abundances are spread over a much wider range. This may reflect the true elemental distribution or simply may be caused by the large associated errors. By means of Fig. 1, we are able to address the key question, whether there is a metallicity gradient in the atmospheres of active stars:

(i) There are strong metallicity gradients in the RS CVn systems II Peg and $\lambda$ And, with the metal abundances being depleted in the corona relative to the photosphere by about one order of magnitude. In the case of II Peg, the Fe gradient is steeper by a factor 2 compared to the Si gradient and possibly also the Mg gradient.

(ii) On the basis of the $1\sigma$-errors, there are weak metallicity gradients in the active single stars $\beta$ Cet and $\pi^1$ UMa, with the metal abundances varying by a factor 2 between photosphere and corona. In both stars, the Fe and Si abundances are depleted, while the Mg abundance is enhanced in the corona relative to the photosphere. This hypothesis can be confirmed with higher significance only if coronal abundances with higher accuracy are available.

In the following, we discuss two possible mechanisms – the 'FIP-effect' and the 'hydrostatic equilibrium stratification' – to explain the observed metallicity gradients.

The concept of the FIP-effect was developed to explain the abundance gradient observed in the solar atmosphere (see Sect. 1). Generally, the FIP-effect denotes the over- or underabundance of elements with a different first ionization potential in the corona relative to the photosphere. On the Sun, the high FIP-elements (N, O, Ne, Ar) are underabundant (relative to H) in the corona by a factor $3-4$ compared to the photosphere, while the low FIP-elements (Fe, Mg, Si, Ca, Na) have the same relative abundances in the photosphere and the corona (Meyer 1985, Feldman & Widing 1990). The metals Fe (FIP $= 7.87$ eV), Mg (FIP $= 7.64$ eV), and Si (FIP $= 8.15$ eV) have essentially the same FIP. Therefore, if the abundance distribution in the stellar atmospheres is determined by the FIP-effect, then all three metals should have 'very similar ratios between their coronal and photospheric abundances. On the basis of the $1\sigma$-errors, the observational results are not consistent with this requirement: II Peg has similar photospheric Fe, Mg, and Si abundances, but the coronal Fe and Si abundances differ by a factor 2. In $\beta$ Cet, the coronal to photospheric abundance ratios of the three metals differ even more: The coronal Fe and Si abundances are depleted by factors 1.4 and 2, while the coronal Mg abundance is enhanced by a factor 1.4 relative to their respective photospheric values. Similarly, in $\pi^1$ UMa the coronal Fe and Si abundances are depleted by factors 2.2 each, while the coronal Mg abundance is enhanced by a factor 1.4 relative to the photospheric values. Thus, the metallicity gradients observed in II Peg, $\beta$ Cet, and $\pi^1$ UMa apparently are not caused by the FIP-effect.

An alternative explanation for the apparent abundance reduction in stellar coronae was proposed recently by Mewe et al. (1997). These authors point out that the coronal metal-depletion may be simply the consequence of hydrostatic equilibrium. Within a coronal loop in hydrostatic equilibrium, the scale height of each ion depends on its mass and charge, and can differ strongly from the mean scale height of the plasma. This dependence may result in an inhomogeneous ion distribution and in reductions of the coronal metal abundances relative to the photospheric abundances by factors $2-10$. To test this hypothesis, we assume to a first approximation that the scale heights of the ions are determined entirely by their mass and neglect the dependence on the charge. With the atomic mass numbers of Fe, Mg, and Si being $56$, $24$, and $28$ amu, the Mg and Si ion stratifications are expected to have about the same scale heights, while the Fe stratification should have a much shorter scale height. Therefore, we expect the coronal to photospheric abundance ratios of Mg and Si to be comparable to each other, while that of Fe should be significantly lower. On the basis of the $1\sigma$-errors, we compare the observed Fe, Mg, and Si stratification with that expected in hydrostatic equilibrium: In II Peg, the coronal abundances are depleted relative to the photospheric ones by a factor $4$ for both Mg and Si, and by a factor $6$ for Fe. Thus, the observed ion stratification roughly corresponds to the one expected in hydrostatic equilibrium. In $\beta$ Cet, the coronal abundances are depleted by factors $2$ and $1.4$ for Si and Fe, but are enhanced by a factor $1.4$ for Mg relative to the photospheric values. In $\pi^1$ UMa, the coronal abundances are depleted by factors $2.2$ for Si and Fe, and are enhanced by a factor $1.4$ for Mg. Thus, in $\beta$ Cet and $\pi^1$ UMa the coronal to photospheric abundance ratios of Fe, Mg, and Si apparently do not follow the hydrostatic equilibrium stratification. Only when in these stars the coronal loops are short compared to the hydrostatic scale height, the coronal abundances are not significantly depleted relative to the photosphere and might scatter around the photospheric values. In this case, the observed Fe, Mg, and Si stratification might not contradict the concept of a hydrostatic equilibrium stratification.

*Acknowledgements.* This project is supported by the Deutsches Zentrum für Luft- und Raumfahrt (DLR), formerly Deutsche Agentur für Raumfahrtangelegenheiten (DARA), under contract 50 OR 9612 0. We thank P. Ballester (ESO) for his kind support with the echelle data reduction, K. Fuhrmann (USM) for his great help in performing the spectral analysis, J. Schmitt, F.-J. Zickgraf and M. Kürster (MPE) for helpful discussions, F. Grupp (USM) for providing us his unpublished Si atomic data, and the referee K. Carpenter for helpful suggestions to improve the paper. This research has made use of the Simbad database, operated at CDS, Strasbourg, France.

## References

Anders E., Grevesse N. 1989, Geochim. Cosmochim. Acta 53, 197.
Bauer F., Bregman J.N. 1996, ApJ 457, 382.
Blackwell D.E., Lynas-Gray A.E. 1994, A&A 282, 899.
Boesgaard A.M., Budge K.G., Burck E.E. 1988, ApJ 325, 749.
Byrne P.B., Panagi P.M., Lanzafame A.C. et al., 1995, A&A 299, 115.
Cayrel R. 1988, in IAU Symp. 132, 345.
Cayrel de Strobel G.C., Bentolila C. 1989, A&A 211, 324.
Dempsey R.C., Neff J.E., O'Neal D., Olah K. 1996, AJ 111, 1356.
Donahue R.A., Saar S.H., Baliunas S.L. 1996, ApJ 466, 384.
Donati J.F., Henry G.W., Hall D.S. 1995, A&A 293, 107.
Dorren J.D., Guinan E.F. 1994, ApJ 428, 805.
Drake S.A., Singh K.P., White N.E., Simon T. 1994, ApJ 436, L87.
ESO-MIDAS User Guide, Vol. B 1995, reference no. MID-MAN-ESO-11000-0003.
Fekel F.C., Balachandran S. 1993, ApJ 403,708.
Feldman U., Widing K.G. 1990, ApJ 363,292.
Fuhrmann K., Axer M., Gehren T. 1993, A&A 271, 451.
Fuhrmann K., Axer M., Gehren T. 1994, A&A 285, 585.
Fuhrmann K., Axer M., Gehren T. 1995, A&A 301, 492.
Fuhrmann K., Pfeiffer M., Frank C., Reetz J., Gehren T. 1997, A&A 323, 909.
Gratton R.G., Ortolani S. 1986, A&A 169, 201.
Gray D.F. 1992, The observation and analysis of stellar photospheres, Cambridge Univ. Press.
Hearnshaw J.B. 1974, A&A 34, 263.
Holweger H., Heise C., Kock M. 1990, A&A 232, 510.
Kovacs N. 1983, A&A 120, 21.
Kurucz R.L. 1979, ApJS 40, 1.
Kurucz R.L. 1995, Highlights of Astronomy 10, 407.
Luck R.E., Challener S.L. 1995, AJ 110, 2968.
Mc William A. 1990, ApJS 74, 1075.
Mewe R., Kaastra J.S., van den Oord G.H.J., Vink J., Tawara Y. 1997, A&A, in press.
Meyer J.P. 1985, ApJS 57, 173.
O'Neal D., Saar S.H., Neff J.E. 1996, ApJ 463, 766.
Pfeiffer M., Frank C., Gehren T. 1998, A&A, in press.
Randich S., Gratton R., Pallavicini R. 1993, A&A 273, 194.
Randich S., Giampapa M.S., Pallavicini R. 1994, A&A 283, 893.
Schrijver C.J., Mewe R., van den Oord G.H.J., Kaastra J.S. 1995, A&A 302, 438.
Singh K.P., White N.E., Drake S.A. 1996, ApJ 456, 766.
Strassmeier K.G. 1990, ApJ 348, 682.
Strassmeier K.G., Hall D.S., Fekel F.C., Scheck M. 1993, A&AS 100, 173.
White N.E., Arnaud K., Day C.S.R. et al., 1994, PASJ 46, L97.
Young A., Ajir F., Thurman G. 1989, PASP 101, 1017.